Semi-metallic polymers

Olga Bubnova, Zia Ullah Khan, Hui Wang, Slawomir Braun, Drew R. Evans, Manrico Fabretto, Pejman Hojati-Talemi, Daniel Dagnelund, Jean-Baptiste Arlin, Yves H. Geerts, Simon Desbief, Dag W. Breiby, Jens W. Andreasen, Roberto Lazzaroni, Weimin Chen, Igor Zozoulenko, Mats Fahlman, Peter J. Murphy, Magnus Berggren and Xavier Crispin

The self-archived postprint version of this journal article is available at Linköping University Institutional Repository (DiVA):
http://urn.kb.se/resolve?urn=urn:nbn:se:liu:diva-104644

N.B.: When citing this work, cite the original publication.
Bubnova, O., Ullah Khan, Z., Wang, H., Braun, S., Evans, D. R., Fabretto, M., Hojati-Talemi, P., Dagnelund, D., Arlin, J., Geerts, Y. H., Desbief, S., Breiby, D. W., Andreasen, J. W., Lazzaroni, R., Chen, W., Zozoulenko, I., Fahlman, M., Murphy, P. J., Berggren, M., Crispin, X., (2014), Semi-metallic polymers, *Nature Materials*, 13(2), 190-194. https://doi.org/10.1038/nmat3824

Original publication available at:
https://doi.org/10.1038/nmat3824

Copyright: Nature Publishing Group
http://www.nature.com/

Tweet

LINKÖPING UNIVERSITY

Semi-metallic polymers

Olga Bubnova[1], Zia Ullah Khan[1], Hui Wang[1], Slawomir Braun[2], Drew R. Evans[7], Manrico Fabretto[7], Pejman Hojati-Talemi[7], Daniel Dagnelund[2], Jean-Baptiste Arlin[3], Yves Geerts[3], Simon Desbief[4], Dag W. Breiby[5], Jens W. Andreasen[6], Roberto Lazzaroni[4], Weimin Chen[2], Igor Zozoulenko[1], Mats Fahlman[2], Peter J Murphy[7], Magnus Berggren[1] and Xavier Crispin[1]*

[1] Linkoping University, Department of Science and Technology, Organic Electronics, SE-601 74 Norrkoping, Sweden
***Email: xavcr@itn.liu.se**

[2] Linköping University, Department of Physics and Measurement Technology, Linköping University, S-581 83 Linköping, Sweden

[3] Free University of Brussels, Laboratoire de Chimie des Polymères, CP 206/1, Boulevard du Triomphe, 1050 Bruxelles, Belgium

[4] University of Mons, Laboratoire de chimie des materiaux nouveaux, Place du Parc 20, B7000 Mons, Belgium

[5] Norwegian University of Science and Technology (NTNU), Department of Physics, Høgskoleringen 5, N-7491 Trondheim, Norway

[6] Technical University of Denmark, Department of Energy Conversion and Storage, Frederiksborgvej 399, 4000 Roskilde, Denmark

[7] University of South Australia, Mawson Institute, Mawson Lakes, 5095, Australia

Polymers are lightweight, flexible, solution-processible materials, which can possess insulating, semiconducting or metallic properties. In addition, because of the high natural abundance of their constituting atoms, polymers are promising materials for low-cost printed electronics, mass produced and/or large-area applications. Semimetals, exemplified by bismuth, graphite and telluride alloys, constitute a class of materials that has no band gap and a very low density of states at the Fermi level. The semimetals have typically higher Seebeck coefficient, lower electrical and thermal conductivities as compared to metals and are utilized in thermoelectric applications. Here, we report that polymers can also be semi-metallic. By comparing the thermoelectric properties of various poly(3,4-ethylenedioxythiophene) (PEDOT) samples, we observe a drastic increase in the Seebeck coefficient when the electrical conductivity is enhanced through molecular organization. This initiates the transition from a Fermi glass to a semimetal. The high Seebeck value, the metallic conductivity at room temperature and the absence of unpaired electron spins makes polymer semimetals attractive for thermoelectrics and spintronics.

Conducting polymers constitute a unique class of materials capable of exhibiting semiconducting and, in some cases, metallic behavior. The resulting electrical conductivity may vary considerably subject to their oxidation level, chain alignment, interchain interactions, conjugation length, degree of disorder etc. In the late 70s copper-like electrical conductivities were reported in polyacetylene films (*1*). The discovery of a soluble

and highly conducting form of polyaniline showing some degree of self-organization led to the first air stable and solution processible metallic polymers (*2, 3*). The electrical conductivity σ increases when cooling down from room temperature and reaches a finite value at 0K. Aside from these examples, most of the conducting polymers are semiconductors at room temperature as characterized by the monotonic decrease in σ as $T \rightarrow 0$. This particular case is well described within the Fermi-glass limit where doping charges do not form extended Bloch energy bands but rather occupy localized states associated with a high degree of local atomic and electronic polarization. Concurrently, in the presence of high disorder the E_F is located within the localized states and transport of charge is governed by temperature-activated hopping (*4*).

Today various conducting polymers routinely reach σ above 1500 S/cm, such as polyaniline (*5*), polypyrrole (*6*) and poly(3,4-ethylenedioxythiophene) PEDOT (*7*). Recently further improvements have been achieved in PEDOT-PSS with an ionic liquid additive (2000 S/cm) (*8*) and an acidic treatment (2500 S/cm) (*9*). The record conductivity value of 3400 S/cm was measured in vapor phase polymerized (VPP) PEDOT-Tos, where Tos stands for the counterion tosylate, using a blend of an oxidant and an amphiphilic copolymer (*10*). Beside transparent electrodes in optoelectronics, numerous new potential applications are emerging. Thermoelectric properties of PEDOT have been optimized through a control of the oxidation level (*11*); as well as through treatment with high boiling point solvent leading to a thermoelectric figure-of-merit equals to ZT=0.42 at room temperature (*12*). These recent breakthroughs bring conducting polymers as attractive low-cost, solution processible and abundant thermoelectric materials compared to the best inorganic bismuth antimony telluride alloys for low temperature applications (*13*). Recently, PEDOT has made its entry in spintronics. An efficient spin-to-charge conversion was demonstrated between a ferromagnetic insulator and PEDOT. Interestingly, the injected spins have a long life time, which is essential to manipulate spins in devices (*14*). Yet, no fundamental explanation has been provided for the high thermoelectric efficiencies and long spin lifetimes in conducting polymers. This motivates a deeper understanding of their electronic structure and morphology.

The conducting polymer chains dissolved in solution show clear modification of their optical properties when their oxidation state is modified (*15*). The removal of electrons from the top of the valence band in a single polymer chain can lead to two different localized positively charged defects: positive polarons (radical cation) and bipolarons (dication) balanced by atomic or molecular counterions. The change in bond length alternation around the excess of positive charge defines the extend of the wavefunction of the (bi)polaron (*16*). This local structural distortion leads to two new in-gap states (i, i*), among which a localized level destabilized from the top of the valence band (VB) (*16, 17*). For a polaron, this level “i” is half-filled (Fig. 1a); while for a bipolaron, it is empty (Fig. 1d). Each of those doping species possesses distinct optical transitions (*15, 16*). A bipolaron has no spin, whereas a polaron possesses a spin of ½ and can be detected by electron spin resonance (*18*).

In the solid state, the polymer chains arrange either in a disorder fashion or self-organize in crystalline domains (*19*). In an amorphous phase, polarons or bipolarons levels are localized on a segment of

the chains. At high oxidation levels, the wavefunction of the charged defects localized on the same chain overlap and a one-dimensional “intra-chain” band is created (*20*). However, this band does not extent through the three dimension of the solid due to disorder and the absence of the inter-chain electronic coupling (*21*). For this reason, in-gap states are spatially localized and spread on an energy distribution. The Fermi level lies among localized states in the middle of the polaron band for a disordered polaronic polymer solid (Fig. 1b); or between the valence band (VB) and the bipolaron band for a disordered bipolaronic polymer solid (Fig 1e) (*22*). Both solids can be considered as Fermi glasses (*23, 24*). In crystalline domains of polymers and in molecular crystals, short inter-chain distances result in an overlap of the π-electronic density of adjacent packed chains; which promotes the delocalization of electronic wavefunction (*25*), such as a polaron spreads on several chains (*26*). Highly oxidized polyaniline can be a metal (*2*) characterized with a half-filled polaron band originating from the creation of a polaron network (Fig. 1c)(*27*). In a first approximation the slope of the density of states (DOS) at E_F is related to the Seebeck coefficient S (*28*). Since the Fermi level is in the middle of a band, metals as well as highly oxidized polyaniline have low thermopower (S<10 μV/K) (*29*). When the degree of disorder decreases, polaronic polymers, such as polyaniline, are known to undergo a transition from Fermi glass to metal (*30*). As far as bipolarons are concerned, the situation is unclear. In contrast to polyaniline, polythiophenes like PEDOT are known to facilitate defects like bipolarons (*31*). Highly oxidized PEDOT possesses up to one charge carrier per three monomer units (*32*). From quantum chemical calculations, a bipolaron in PEDOT spreads over six monomer units or more (*33*). However, no clear picture of the band structure is proposed for semi-crystalline bipolaronic polymers and none has demonstrated the possibility to create a network of bipolaron in a polymer solid. Herein, we demonstrate metallic transport at room temperature in a bipolaron network created in polycrystalline PEDOT. In contrast to metals and metallic polyaniline, we measure a large S in PEDOT indicating its semi-metallic character.

PEDOT samples with different σ spreading over six orders of magnitudes are prepared. The PEDOT-PSS films are obtained by drop casting of PEDOT-PSS water emulsions to which diethylene glycol (DEG) is added in different amounts (*34*). The room temperature σ is ~0.007 S/cm, ~0.02 S/cm, ~1.1 S/cm and ~10 S/cm for PEDOT-PSS with 0%, 0.05%, 0.5%, 5% DEG respectively. DEG as well as many other polar solvents enhances the electrical conductivity through a morphology change (*35, 36*) or a modification in the chain packing (*37*) (Fig. S1), with no effect on the oxidation level (Fig. S2). An electrical conductivity of 500 S/cm is measured in PEDOT with tosylate (Tos) counterion. PEDOT-Tos is prepared by chemical polymerization (see supplementary information) (*38*). To further enhance the conductivity, we use a vapor phase polymerization technique to fabricate PEDOT-Tos films which are templated by glycol based triblock copolymers (PEG-PPG-PEG)(*39*). The measured conductivity is 800 S/cm, 1200 S/cm, and 1500 S/cm for the copolymer with a molecular weight of 2900M_w, 5800Mw with DMF as an added solvent and 5800Mw without DMF.

Grazing incidence X-ray scattering (GIWAXS) has become a frequently used tool for the structural characterization of polymers, including PEDOT (*40-42*). GIWAXS patterns for the various PEDOT samples are

displayed in Fig. 2. All the PEDOT-PSS samples are essentially amorphous, or "weakly ordered polymer aggregates". The broad peak at ~1.70 $Å^{-1}$ is ascribed to intermolecular ordering of PEDOT chains, presumably involving π-stacking (Fig. 2a). Already with a minor addition of 0.05% DEG to the PEDOT-PSS, another broad peak at Q ~1.25 Å-1 (d = 5 Å) appears (Fig. 2b), presumably from separated PSS domains (*43*). Some preferred orientation is present in the PEDOT-PSS samples with the π-stacking tending to be out-of-plane. The PEDOT-Tos sample, Fig. 2c, exhibits several sharp diffraction peaks, making this sample qualitatively different from the PEDOT-PSS samples. A likely interpretation of the scattering patterns is that the material contains well-ordered crystallites separated from each other by a less-ordered "amorphous" matrix. The orthorhombic unit cell suggested for PEDOT-Tos with a = 14.0 Å, b = 6.8 Å and c = 7.8 Å (*44*), having the polymer chain axes parallel to the c-axis, accounts fairly well for the experimental peak positions when assuming that the unit cell is highly oriented (FWHM < 10°) with the a-axis perpendicular to the substrate. This model indicates the formation of lamella of π-stacked PEDOT chains separated by an inter-lamella space occupied by Tos (*40, 43*). However, the experimental scattering pattern shows pronounced off-axis scattering (at χ~40° with respect to the substrate plane) with high intensity at the corresponding *201* (Q = 1.21 $Å^{-1}$) and *210* (Q = 1.29 $Å^{-1}$) Bragg peaks which cannot be explained by this model, suggesting that the band-shaped polymer chains in the present case are not fully edge-on with respect to the substrate plane.

The density-of-valence-electronic-states (DOVS) can be probed by ultraviolet photoelectron spectroscopy (UPS). The UPS spectra of PEDOT-PSS 5%DEG and PEDOT-Tos are displayed in Fig. 3a,b. Close to E_F, the UPS spectrum of PEDOT-PSS shows an abrupt decay at 1.5 eV followed by a smooth tail reaching E_F. Only π-electrons contribute to the signal in that binding energy range. This tail is associated with the presence of localized filled states induced by disorder. The amorphous PEDOT-PSS is a Fermi glass. The PEDOT-Tos UPS spectrum displays a large DOVS at E_F and a totally different shape without a disorder-induced tail. PEDOT-Tos with lower work function (4.3 eV) as compared to PEDOT-PSS (5.1 eV) has the valence band closer to E_F. A significant background absorption in the IR is recorded for PEDOT-Tos (see Fig S2) down to <0.05 eV implying a vanishingly small band gap well below the resolution of the photoelectron spectrometer.

Electron paramagnetic resonance (EPR) detects the presence of unpaired electrons in solids (*45*). The EPR spectra for the various PEDOT samples are depicted in Fig. 3c. The addition of the secondary dopant, which leads to an increase in σ, systematically diminishes the paramagnetic signal. In PEDOT-PSS, the fraction of spin per monomer equals to 2.3% (3.27×10^{16} spin/mm^3), 2.2%, 1.2% and 0.33% for PEDOT-PSS with 0%, 0.05%, 0.5% and 5% DEG, respectively. Based on a carrier density of about 33% per monomer (*32, 45, 46*), PEDOT-PSS contains 7% of polarons and 93% bipolarons. The ratio depends on DEG, which likely promotes the pairing of polarons into bipolarons. The remaining EPR signal is intrinsically related to the molecular disorder that impedes the coupling of the remaining polarons to other charged defects. Surprisingly, the

polycrystalline PEDOT-Tos shows no ESR signal at all, indicating that polaron pairs (*33*) or bipolarons are the only type of charge carriers.

The Seebeck coefficient S versus electrical conductivity σ is reported for various PEDOT samples at 300K (Fig. 4a). Two main trends can be distinguished: (i) S is almost constant for all PEDOT-PSS samples despite the large variation in σ; (ii) S increases drastically for highly conducting PEDOT-Tos samples up to 55 μV/K for 1500 S/cm. This cannot be attributed to different doping levels[*], as it would lead to an opposite behavior (large S - low σ) (*11, 47*). Interestingly, σ vs. T (Fig. 4b) indicates two regimes as well: (i) a semiconducting behaviour with positive temperature coefficient, i.e. a thermally activated transport for PEDOT-PSS; and, (ii) a metallic behaviour for PEDOT-Tos with negative temperature coefficient at room temperature, which was previously observed only below 10K (46). Hence, the regime of charge transport and the value of the Seebeck show an unexpected correlation. The difference in slope for the metallic σ vs. T for the various PEDOT-Tos samples indicates that two modes of transport are active simultaneously with different weight: metallic and hopping conductions. The larger the metallic contribution, the higher the conductivity and, surprisingly, the same applies to the Seebeck coefficient. The large S of PEDOT-Tos as compared to polyaniline (<10 μV/K) and other metals suggests that it is not a metal but a semi-metal. We therefore propose that the electronic structure of PEDOT-PSS can be described by a Fermi glass as indicated in Fig. 1e, whereas PEDOT-Tos is defined by what looks more like a bipolaron network with an empty delocalized bipolaron band merging into the delocalized valence band, cf. Fig. 1f.

[*] The effect of the difference in doping level for the samples is further ruled out by the following facts: (i) the measured oxidation level in PEDOT-Tos (0.36%|e|/monomer unit) is similar (or slightly higher) than in PEDOT-PSS (0.33|e|/monomer unit) (46). (ii) The thermopower varies most for the various PEDOT-Tos samples while the oxidant used during the synthesis is the same; that is the oxidation level is likely identical.

With this model in mind, we come back to the interpretation of the S evolution (Fig. 1a). Mott's formula (*48*), which is valid for both hopping and band motion transport mechanisms, states that S is proportional to $[d(\ln\sigma(E))/dE]$ at E_F. Since the energy dependence of the conductivity is primarily determined by the density of state N(E), the Seebeck coefficient is therefore proportional to $S \div [d(\ln N(E))/dE]_{E=EF}$. In the amorphous bipolaron system (Fig. 1e), E_F lays in the localized states fading out from the valence and bipolaron bands. As supported by the UPS data, the DOS at E_F is not varying much and is close to its minimum, which explains the low value of S of PEDOT-PSS. For PEDOT-Tos, E_F is in a strongly varying DOS region (Fig. 1f), such that $[d(\ln N(E))/dE]_{E=EF}$ and S are larger. Note that the DOS asymmetry is amplified with structural order as the localized levels smooth out the DOS. This explains the larger S for PEDOT-Tos with high σ. It is clear that further improvement in structural order (higher σ) should in principle result in even larger *S* and thus thermoelectric power factor σS^2. In disordered or metallic polyaniline with polarons as major doping species, E_F is in a slowly varying region of the DOS (Fig. 1b and 1c). Hence conducting polymers composed of a bipolaron network (semimetallic) are expected to have better thermoelectric properties than those with a polaron network (metallic). Finally, the absence of (residual) polarons in semimetallic PEDOT-Tos is a unique feature that can be exploited in spintronics, since the absence of unpaired electrons in the solid prevents the spin scattering and increases the spin life time.

ACKNOWLEDGMENTS

The authors acknowledge the European Research Council (ERC-starting-grant 307596), the Swedish foundation for strategic research (project: "Nano-material and Scalable TE materials"), the Knut and Alice Wallenberg foundation (project "Power paper"), The Swedish Energy Agency and the Advanced Functional Materials Center at Linköping University. Research in Mons is supported by the European Commission and Région Wallonne (FEDER 'Revêtements Fonctionnels' program), BELSPO (IAP 7/05), the OPTI2MAT Excellence program of Région Wallonne, and FNRS-FRFC. Research at the University of South Australia is supported by ITEK, the commercialization company for UniSA. Research at NTNU is supported by the Norwegian Research Council.

References:

1. C. K. Chiang *et al.*, Electrical Conductivity in Doped Polyacetylene. *Physical Review Letters* **39**, 1098 (1977).
2. K. Lee *et al.*, Metallic transport in polyaniline. *Nature* **441**, 3 (2006).
3. Y. Cao, G. M. Treacy, P. Smith, A. J. Heeger, Solution-cast films of polyaniline: Optical-quality transparent electrodes. *Applied Physics Letters* **60**, 2711 (1992).
4. S. Wang, M. Ha, M. Manno, C. Daniel Frisbie, C. Leighton, Hopping transport and the Hall effect near the insulator-metal transition in electrochemically gated poly(3-hexylthiophene) transistors. *Nature Communications* **3**, (2012).

5. S. J. Pomfret, P. N. Adams, N. P. Comfort, A. P. Monkman, Inherently Electrically Conductive Fibers Wet Spun from a Sulfonic Acid–Doped Polyaniline Solution. *Advanced Materials* **10**, 1351 (1998).
6. M. Yamaura, T. Hagiwara, K. Iwata, Enhancement of electrical conductivity of polypyrrole film by stretching: Counter ion effect. *Synthetic Metals* **26**, 209 (1988).
7. M. Fabretto *et al.*, High conductivity PEDOT resulting from glycol/oxidant complex and glycol/polymer intercalation during vacuum vapour phase polymerisation. *Polymer* **52**, 1725 (2011).
8. C. Badre, L. Marquant, A. M. Alsayed, L. A. Hough, Highly Conductive Poly(3,4-ethylenedioxythiophene):Poly (styrenesulfonate) Films Using 1-Ethyl-3-methylimidazolium Tetracyanoborate Ionic Liquid. *Advanced Functional Materials* **22**, 2723 (2012).
9. Y. Xia, K. Sun, J. Ouyang, Solution-Processed Metallic Conducting Polymer Films as Transparent Electrode of Optoelectronic Devices. *Advanced Materials* **24**, 2436 (2012).
10. M. V. Fabretto *et al.*, Polymeric Material with Metal-Like Conductivity for Next Generation Organic Electronic Devices. *Chemistry of Materials* **24**, 3998 (2012/10/23, 2012).
11. O. Bubnova *et al.*, Optimization of the thermoelectric figure of merit in the conducting polymer poly(3,4-ethylenedioxythiophene). *Nat Mater* **10**, 429 (2011).
12. T. Park, C. Park, B. Kim, H. Shin, E. Kim, Flexible PEDOT electrodes with large thermoelectric power factors to generate electricity by the touch of fingertips. *Energy & Environmental Science*, (2013).
13. Q. H. Bed Poudel, Yi Ma, Yucheng Lan, Austin Minnich, Bo Yu, Xiao Yan, Dezhi Wang, Andrew Muto, Daryoosh Vashaee, Xiaoyuan Chen, Junming Liu, Mildred S. Dresselhaus, Gang Chen, and Zhifeng Ren, High-Thermoelectric Performance of Nanostructured Bismuth Antimony Telluride Bulk Alloys. *Science* **320**, 4 (2008).
14. K. Ando, S. Watanabe, S. Mooser, E. Saitoh, H. Sirringhaus, Solution-processed organic spin–charge converter. *Nat Mater* **12**, 622 (2013).
15. K. Jeuris, L. Groenendaal, H. Verheyen, F. Louwet, F. C. De Schryver, Light stability of 3,4-ethylenedioxythiophene-based derivatives. *Synthetic Metals* **132**, 289 (2003).
16. J. Cornil, D. Beljonne, J. L. Bredas, Nature of optical transitions in conjugated oligomers. I. Theoretical characterization of neutral and doped oligo(phenylenevinylene)s. *The Journal of Chemical Physics* **103**, 834 (1995).
17. J. L. Brédas, F. Wudl, A. J. Heeger, Polarons and bipolarons in doped polythiophene: A theoretical investigation. *Solid State Communications* **63**, 577 (1987).
18. F. Devreux, F. Genoud, M. Nechtschein, B. Villeret, ESR investigation of polarons and bipolarons in conducting polymers:: the case of polypyrrole. *Synthetic Metals* **18**, 89 (1987).
19. D. C. Martin *et al.*, The Morphology of Poly(3,4-Ethylenedioxythiophene). *Polymer Reviews* **50**, 340 (2010/07/27, 2010).
20. S. Stafström, J. L. Brédas, Evolution of the electronic structure of polyacetylene and polythiophene as a function of doping level and lattice conformation. *Physical Review B* **38**, 4180 (1988).
21. V. N. Prigodin, K. B. Efetov, Localization transition in a random network of metallic wires: A model for highly conducting polymers. *Physical Review Letters* **70**, 2932 (1993).
22. F. C. Lavarda, M. C. dos Santos, D. S. Galvão, B. Laks, Insulator-to-metal transition in polythiophene. *Physical Review B* **49**, 979 (1994).
23. N. S. Sariciftci, A. J. Heeger, Y. Cao, Paramagnetic susceptibility of highly conducting polyaniline: Disordered metal with weak electron-electron interactions (Fermi glass). *Physical Review B* **49**, 5988 (1994).

24. A. J. Heeger, Semiconducting and Metallic Polymers: The Fourth Generation of Polymeric Materials (Nobel Lecture). *Angewandte Chemie International Edition* **40**, 2591 (2001).
25. G. Koller *et al.*, Intra- and Intermolecular Band Dispersion in an Organic Crystal. *Science* **317**, 351 (2007).
26. D. Beljonne *et al.*, Optical Signature of Delocalized Polarons in Conjugated Polymers. *Advanced Functional Materials* **11**, 229 (2001).
27. S. Stafström *et al.*, Polaron lattice in highly conducting polyaniline: Theoretical and optical studies. *Physical Review Letters* **59**, 1464 (1987).
28. G. J. Snyder, Toberer, Eric S., Complex thermoelectric materials. *Nature materials* **7**, 9 (2008).
29. N. Mateeva, H. Niculescu, J. Schlenoff, L. R. Testardi, Correlation of Seebeck coefficient and electric conductivity in polyaniline and polypyrrole. *Journal of Applied Physics* **83**, 3111 (1998).
30. C. O. Yoon *et al.*, Hopping transport in doped conducting polymers in the insulating regime near the metal-insulator boundary: polypyrrole, polyaniline and polyalkylthiophenes. *Synthetic Metals* **75**, 229 (1995).
31. A. Zykwinska, W. Domagala, A. Czardybon, B. Pilawa, M. Lapkowski, In situ EPR spectroelectrochemical studies of paramagnetic centres in poly(3,4-ethylenedioxythiophene) (PEDOT) and poly(3,4-butylenedioxythiophene) (PBuDOT) films. *Chemical Physics* **292**, 31 (2003).
32. G. Zotti *et al.*, Electrochemical and XPS Studies toward the Role of Monomeric and Polymeric Sulfonate Counterions in the Synthesis, Composition, and Properties of Poly(3,4-ethylenedioxythiophene). *Macromolecules* **36**, 3337 (2003/05/01, 2003).
33. V. M. Geskin, J.-L. Brédas, Polaron Pair versus Bipolaron on Oligothiophene Chains: A Theoretical Study of the Singlet and Triplet States. *ChemPhysChem* **4**, 498 (2003).
34. X. Crispin *et al.*, The Origin of the High Conductivity of Poly(3,4-ethylenedioxythiophene)−Poly(styrenesulfonate) (PEDOT−PSS) Plastic Electrodes. *Chemistry of Materials* **18**, 4354 (2006/09/01, 2006).
35. S. K. M. Jonsson *et al.*, The effects of solvents on the morphology and sheet resistance in poly (3,4-ethylenedioxythiophene)-polystyrenesulfonic acid (PEDOT-PSS) films. *Synthetic Metals* **139**, 1 (Aug, 2003).
36. R. A. J. J. A. M. Nardes, and M. Kemerink, *Advanced Functional Materials* **18**, 865 (2008).
37. B. H. L. N. Kim, D. Choi, G. Kim, H. Kim, J.-R. Kim, J. Lee, Y. H. Kahng, and K. Lee., *Physical Review Letters* **109**, 106405 (2012).
38. B. Winther-Jensen, K. West, Vapor-Phase Polymerization of 3,4-Ethylenedioxythiophene: A Route to Highly Conducting Polymer Surface Layers. *Macromolecules* **37**, 4538 (2004/06/01, 2004).
39. D. Evans *et al.*, Structure-directed growth of high conductivity PEDOT from liquid-like oxidant layers during vacuum vapor phase polymerization. *Journal of Materials Chemistry* **22**, 14889 (2012).
40. B. Winther-Jensen *et al.*, Order–disorder transitions in poly(3,4-ethylenedioxythiophene). *Polymer* **49**, 481 (2008).
41. B. Winther-Jensen *et al.*, High current density and drift velocity in templated conducting polymers. *Organic Electronics* **8**, 796 (2007).
42. D. W. Breiby, E. J. Samuelsen, L. B. Groenendaal, B. Struth, Smectic structures in electrochemically prepared poly(3,4-ethylenedioxythiophene) films. *Journal of Polymer Science Part B: Polymer Physics* **41**, 945 (2003).
43. N. Kim *et al.*, Role of Interchain Coupling in the Metallic State of Conducting Polymers. *Physical Review Letters* **109**, 106405 (2012).

44. K. E. Aasmundtveit *et al.*, Structure of thin films of poly(3,4-ethylenedioxythiophene). *Synthetic Metals* **101**, 561 (1999).
45. W. Domagala, B. Pilawa, M. Lapkowski, Quantitative in-situ EPR spectroelectrochemical studies of doping processes in poly(3,4-alkylenedioxythiophene)s: Part 1: PEDOT. *Electrochimica Acta* **53**, 4580 (2008).
46. X. Crispin *et al.*, Conductivity, morphology, interfacial chemistry, and stability of poly(3,4-ethylene dioxythiophene)-poly(styrene sulfonate): A photoelectron spectroscopy study. *Journal of Polymer Science Part B-Polymer Physics* **41**, 2561 (Nov, 2003).
47. O. Bubnova, M. Berggren, X. Crispin, Tuning the Thermoelectric Properties of Conducting Polymers in an Electrochemical Transistor. *Journal of the American Chemical Society* **134**, 16456 (2012/10/10, 2012).
48. M. Cutler, N. F. Mott, Observation of Anderson Localization in an Electron Gas. *Physical Review* **181**, 1336 (1969).

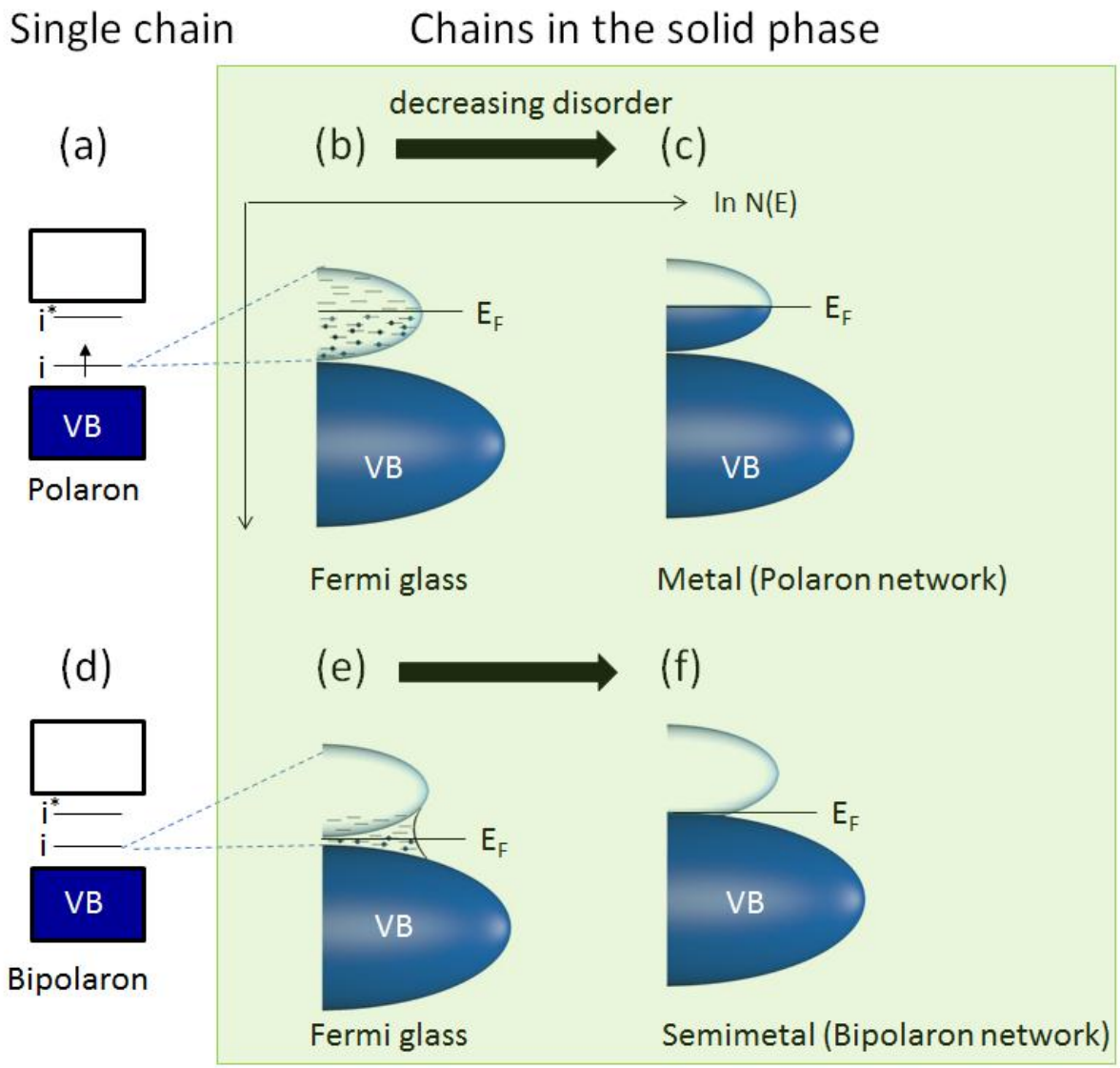

Fig. 1. Electronic structure of conducting polymers

Electronic structure of a polymer chain with (a) one polaron and (d) one bipolaron on a single polymer chain. Sketch of the logarithm of the density of state ln N(E) for an amorphous (b) polaronic and (e) bipolaronic polymer solid with localized states around the Fermi level E_F; as well as for (c) a metallic network of polarons (metal) and (f) a semi-metallic network of bipolarons with the Fermi level lying in a delocalized band.

Fig. 2. Structure of various PEDOT thin films

GIWAXS patterns obtained for : (a) PEDOT-PSS (without DEG), showing only a broad peak near Q = 1.70 Å-1 (d ~ 3.7 Å) which is related to interchain stacking. (b) PEDOT-PSS 0.05% DEG, showing a broad additional peak at Q = 1.25Å-1 (d ~ 5.0 Å) which we ascribe to PSS domains. (c) PEDOT-Tos, being qualitatively different from the PEDOT-PSS samples with several sharp diffraction rings. The superimposed semicircles give the values for the scattering vector Q in units of Å-1, with values as indicated in (a). The horizon, corresponding to in-plane scattering, is also indicated. The shadow on the left-hand side, seen in (a) and (b), is an experimental artifact.

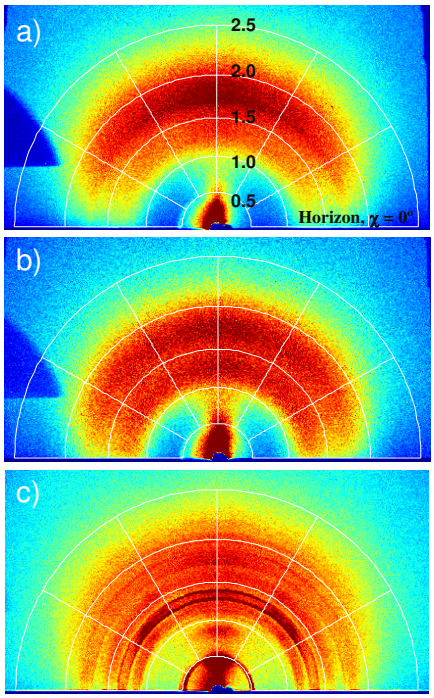

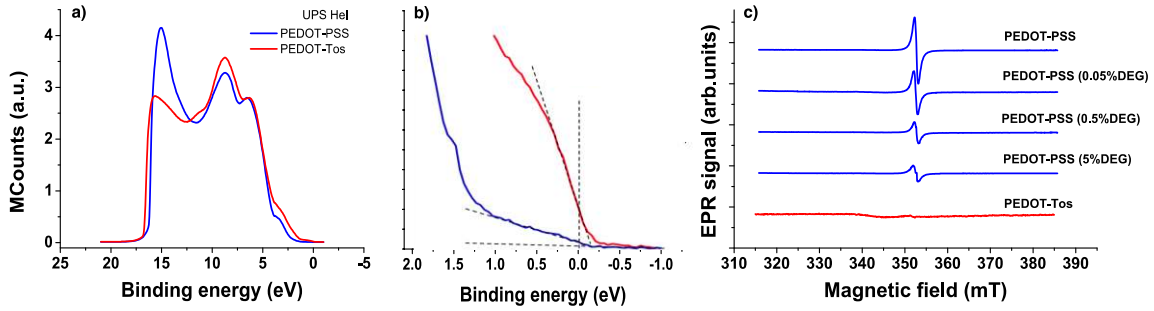

Fig 3. Electronic valence levels and nature of the charge carriers

(a) UPS valence band spectra (HeI radiation) of PEDOT-PSS and PEDOT-Tos (blue curve and red curve, respectively). (b) The magnified view of the low binding energy region shows the DOVS of PEDOT-PSS and PEDOT-Tos; (c) EPR spectra of untreated (strongest signal) and DEG-treated PEDOT-PSS films, PEDOT-Tos shows no EPR signal.

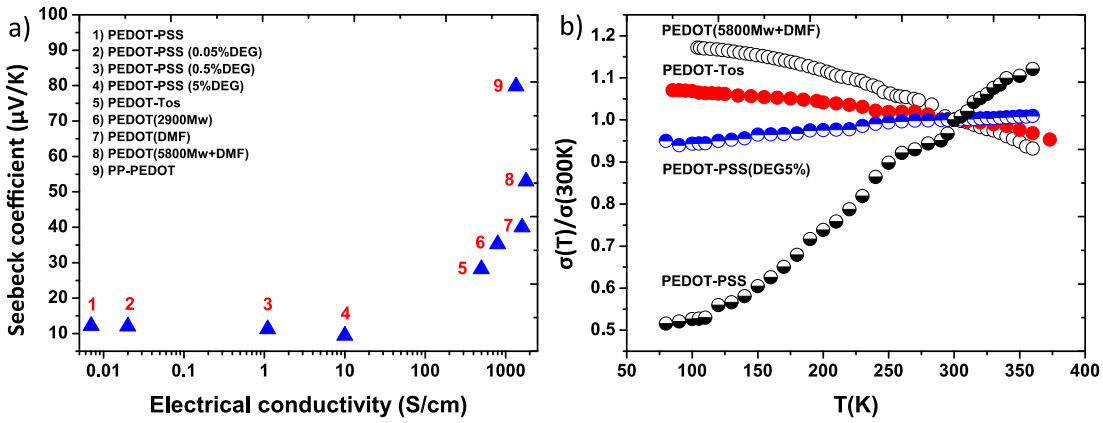

Fig 4. Thermopower and electrical conductivity of PEDOT derivatives

(a) Seebeck coefficient versus electrical conductivity of various PEDOT derivatives including pristine PEDOT-PSS and DEG containing samples, chemically polymerized PEDOT-Tos as well as three VPP PEDOT-Tos with tri-block copolymers poly(ethylene glycol–propylene glycol– ethylene glycol) (PEG–PPG–PEG) with different Mw. The point ▲9 is coming from ref. (*1*); i.e. not using the same set-up to measure the Seebeck coefficient. (b) Temperature dependence of the electrical conductivity of the chemically polymerized PEDOT-Tos and VPP PEDOT 5800Mw.

Supplementary Materials for

Semi-metallic polymers

Olga Bubnova, [1] Zia Ullah Khan, [2] Hui Wang, Slawomir Braun [3,] Drew R. Evans, Manrico Fabretto, Pejman Hojati-Talemi, Daniel Dagnelund, Jean-Baptiste Arlin, Yves Geerts, Simon Desbief, Dag W. Breiby, Jens W. Andreasen, Roberto Lazzaroni, Weimin Chen, Igor Zozoulenko, Mats Fahlman, Peter J Murphy, Magnus Berggren and Xavier Crispin*

correspondence to: xavcr@liu.se

1. Morphology and structure

The surface morphology of PEDOT-Tos and PEDOT-PSS is characterized by atomic force microscopy (AFM). Fig. S1 displays 500x500nm^2 height and phase images recorded in tapping-mode. The phase signal is related to the interaction of the oscillating tip with the sample surface, and is routinely employed to qualitatively observe spatial differences in the surfaces local mechanical properties and/or adhesion of the tip to the surface. The morphology of PEDOT-Tos (Fig. S1a, left) shows circular grains, of a mean diameter of 20 nm, which are aggregated in a compact manner. The phase image reveals a rather homogeneous chemical composition, as indicated by only small variations in phase angle and a one-to-one correspondence with the topographic profile. The surface of PEDOT-PSS (Fig. S1b) is smooth but the phase image reveals the presence of elongated structures approximately 7 nm wide, most probably coming from a slight phase separation between PEDOT-PSS and the excess of PSS. The brighter islands on the phase image correspond to harder material and can be attributed to highly conducting PEDOT regions, whereas the dark features are related to softer areas, presumably PSS-rich zone (as PSS is hygroscopic, absorption of water can soften it). PEDOT-PSS is composed of three times more PSS than PEDOT(*1*) and PEDOT-PSS films are known to have a high content of PSS at the surface(*2*).The introduction of DEG further favors the phase separation of the excess of PSS, leading to irregular large domains (>20nm) (Fig. S1c), while the highly conductive PEDOT-PSS organizes in a three-dimensional network. The electrical conductivity of PEDOT-PSS at room temperature increases from ~0.007 S/cm for PEDOT-PSS, to ~0.02 S/cm, ~1.1 S/cm and ~10 S/cm with 0.05%, 0.5%, 5% DEG. DEG as well as many other polar solvents are called secondary-dopants because they significantly enhance the electrical conductivity through a morphology change(*3*) or a modification in the packing of PEDOT chains (33), as depicted in the AFM images (Fig. S1) and GIWAXS data (Fig. 1a and b), rather than through a variation of the oxidation level (primary dopant)(34) as indicated by the similar absorption spectra for various DEG content (Fig. S3).

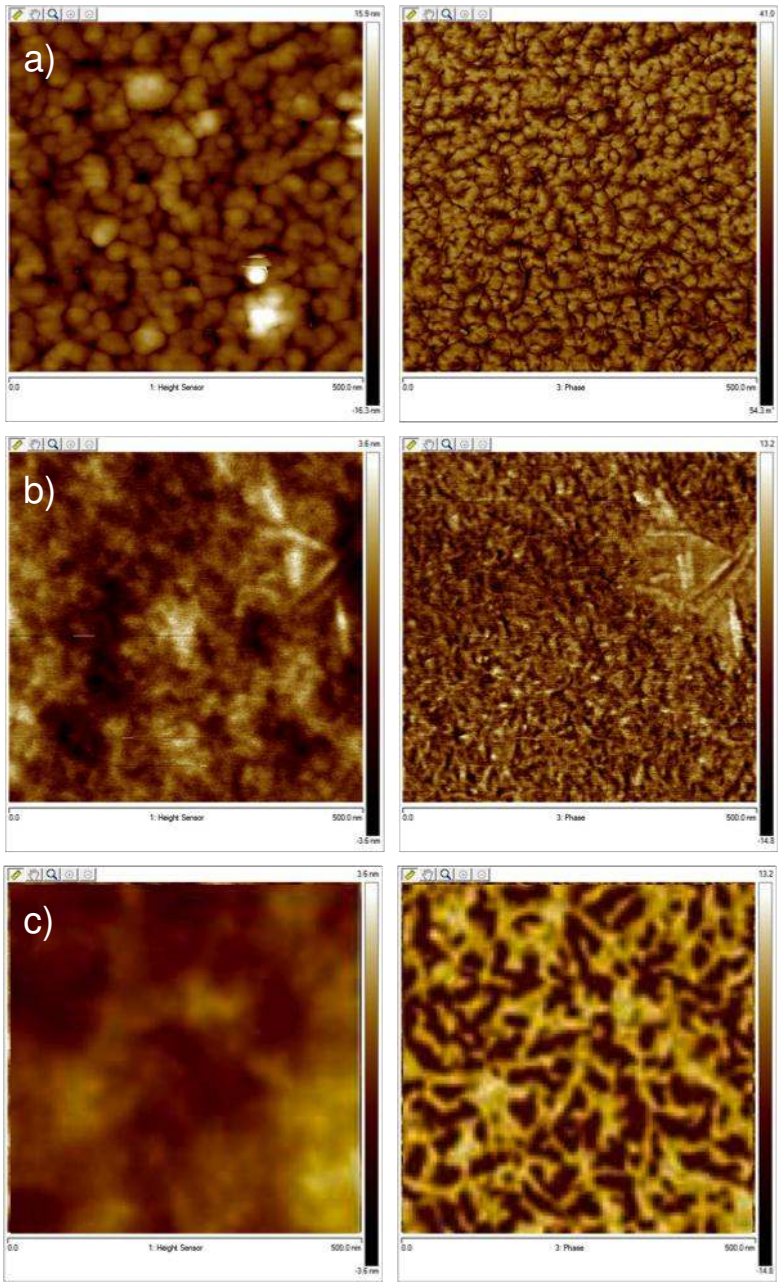

Fig S1. 500x500nm^2 topography (left) and phase (right) AFM images of a) Pedot-Tos b) Pedot-Pss (the vertical scale is 7nm for the image on the left and 30° for the right image) and c) Pedot-Pss with 5wt% DEG (image c) is after (*3*)

In order to distinguish further differences between PEDOT-Tos and PEDOT-PSS, the materials were characterized by polarized optical microscopy (POM). With cross-polarizers, no light could pass through the PEDOT-PSS samples (Fig. S2a), which indicates that the films are globally amorphous and isotropic. In contrast, a clear birefringence is observed with PEDOT-Tos (Fig. 2Sd) suggesting the presence of semi-crystalline PEDOT domains. The pattern

observed in the POM images is due to the granular like morphology, with grains of about 20 μm diameter.

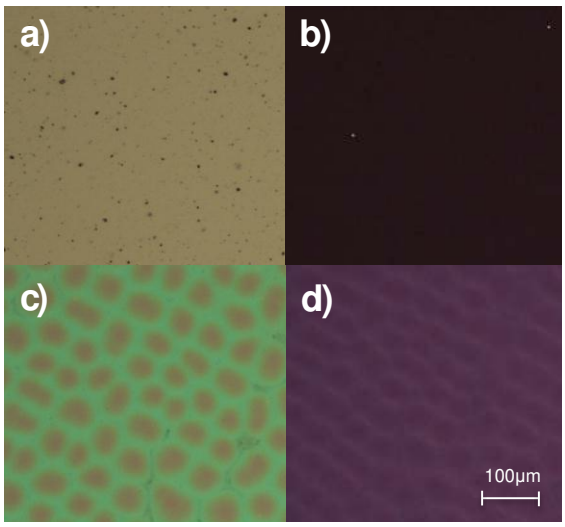

Fig. S2. Polarized optical microscopy (POM) images of PEDOT-PSS and PEDOT-Tos films: (a) and (c) aligned polarizes; (b) and (d) - crossed polarizers

2. Absorption spectroscopy

All PEDOT samples possess a vanishingly small optical band gap as illustrated by the broad optical absorption in the infrared (Fig. S3). There is however, a major difference between the amorphous PEDOT-PSS samples and PEDOT-Tos. The absorption in PEDOT-PSS is almost constant in the range 1000-2500nm, and slightly increases at long wavelengths with the addition of DEG. The optical absorption in the amorphous PEDOT is associated to band transitions between localized levels in the valence band edge and bipolaronic bands or localized levels. Similar effect has been observed for polyaniline(*4*) (*5*) in the case of polaronic bands. PEDOT-Tos absorbs less intensively in the visible as compared to PEDOT-PSS as it has no or very little neutral PEDOT segments and the charge carrier wavefunctions are delocalized (Fig. S3a). Its absorption background in the IR is much more pronounced and continuously increases towards low energies. The absorption of PEDOT-Tos in the IR extends below 0.05eV (see Fig. S3b). This result is possible if some occupied levels of the valence band overlap with the delocalized bipolaron band, thus allowing partial occupation of the later. We believe this is a second indication that PEDOT-Tos is a semimetal.

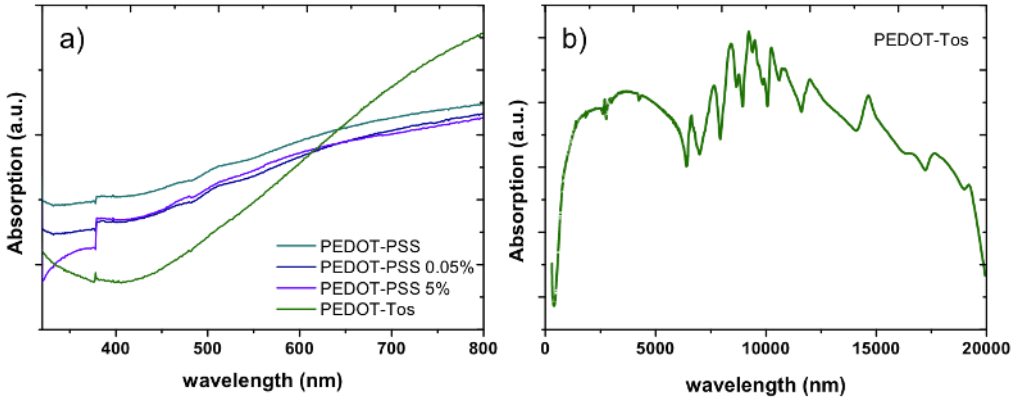

Fig S3. a) Optical absorption of PEDOT-Tos and PEDOT-PSS with various DEG content. The absorbance has been normalized with respect to the polymer films thickness. b) FTIR spectrum of PEDOT-Tos

3. Experimental methods

Sample preparation

PEDOT-Tos films were obtained by chemical polymerization from a mixture of 1 ml of Baytron C (iron (III)-tosylate in butanol) and 50µl of EDOT monomer provided by Sigma-Aldrich. The solution was spin coated on a glass substrate at 1000rpm for 30 seconds yielding 100-150nm thick films, the coating was then annealed at 60°C for 10 minutes and carefully rinsed with DI water several times to remove unreacted oxidant. PEDOT-PSS film was prepared directly by depositing (a 1.2% PEDOT-PSS water emulsion provided by Agfa Geveart) on glass by drop casting which was followed by annealing in the oven at about 60°C for 15 minutes. Three more samples with different amount of DEG (0.05w%, 0.5w% and 5w% in the PEDOT-PSS emulsion) were prepared in a similar manner.

Higher conductivity PEDOT-Tos samples were prepared using the vapor phase polymerization technique, where triblock copolymer was used to template the growth. Three variants were made, using different PEG-PPG-PEG copolymers and/or additional solvents. Each oxidant solution was prepared by diluting from the Baytron C stock solution, as used in the chemical polymerization. The sample labeled PEDOT-Tos(2900Mw) was prepared from an oxidant solution containing 13 wt% PEG-PPG-PEG of 2900Mw and 13.9 wt% iron (III)-tosylate in butanol. The other two samples were prepared using an oxidant solution with 12.3 wt% iron (III)-tosylate and the PEG-PPG-PEG copolymer of 5800Mw at 23 wt%, with either (i) butanol, labeled PEDOT-Tos(5800Mw) or (ii) a dimethyl formamide/butanol blend, labeled PEDOT-Tos(5800Mw + DMF). Each oxidant solution was spin-coated on a glass substrate at 1500rpm for 25 seconds, heated at 70°C for 30 seconds, then exposed to the EDOT monomer in a vacuum oven (45mbar, 35°C) for 25 minutes. The resulting PEDOT-Tos films were washed using ethanol to remove

any unreacted oxidant.

Thermoelectric measurement

The set up for the Seebeck coefficient measurement consisted (see Fig S4) of two aluminum blocks, 25mm separated from each other. One of the blocks was heated, while the other one was kept at room temperature. Two glass slides "Sample" with polymer film and "Reference" with calibrated gold thermistors were fixed between the hot and cold sides. The Au lines were 35μm wide with four pads, each being 0.5mm in diameter. The polymer was spin coated on the "Sample" glass slide while SU-8 was deposited on the reference glass to compensate for the heat transported through the conducting polymer. Both glass slides were tightly fixed between the two aluminum blocks of different temperature to ensure a good thermal contact within the set-up. The resistances of the two thermistors on the reference sample were measured with the four-point probe method using a Keithley 2400, and the temperature difference between two lines was subsequently calculated from the respective calibration slopes. The generated thermoelectric voltage (ΔV) was measured with a nanovoltmeter Keithley 2200, with one probe each on the hot and cold Au lines joined by the polymer film in between. The Seebeck coefficient was calculated as ΔV/ ΔT. All the values were subsequently corrected by subtracting the absolute Seebeck coefficient of gold. The electrical conductivities of all five samples were measured by means of the four-point probe method which is described elsewhere(*6*). The temperature dependence measurements were conducted using the set-up described in Fig S4. The temperature on the film was calculated by averaging signals recorded from two thermistors located on the reference sample. The temperature gradient was measured in the same manner. The Seebeck coefficient and the electrical conductivity were measured as described above.

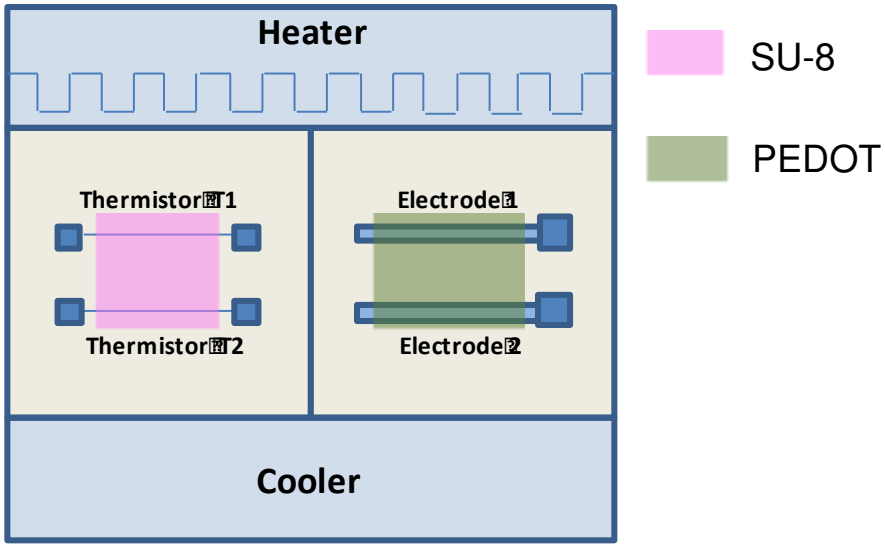

Fig S4. Schematic of the Seebeck coefficient measurement set-up

AFM

Morphological AFM measurements were performed using a Dimension Icon microscope equipped with a Nanoscope V controller from Bruker-Nano. All images were recorded under ambient conditions. In Intermittent Contact AFM (tapping-mode) mode, Si cantilevers with a resonance frequency in the 150-300 kHz range are used. All the measurements are done with the scan size of 500x500nm2.

GIWAXS

Grazing Incidence Wide-Angle X-ray Scattering (GIWAXS) experiments were performed on a custom-built setup at Risoe, based on a rotating Cu-anode from Rigaku, equipped with a 1D multilayer mirror from Xenocs yielding parallel and monochromatic X-ray Cu Kα radiation (wavelength λ = 1.5418 Å). The incidence angle used was 0.20°, near the critical angle for the glass substrates. The measurements were done in vacuum, at room temperature. The scattered radiation was collected using a Fuji imaging plate placed at 119 mm from the sample. All the GIWAXS patterns are represented as raw-data with superposed semi-circles indicating isovalues (0.5, 1.0, 1.5, 2.0 and 2.5) $Å^{-1}$ of the magnitude $Q = 4\pi\sin(\theta) / \lambda$ of the scattering vector **Q**. The angle θ is half the total scattering angle 2θ. Note that while the horizon in the GIWAXS patterns correspond to in-plane scattering, the vertical direction in the patterns does *not* correspond to specular scattering, as the scattering vector will have an in-plane component also for this geometry. Note that a limitation of the GIWAXS technique, in particular as carried out in home laboratories with less well-defined collimation, is that the long "footprint" of the beam on the sample, arising from the grazing incidence angle, precludes investigating the crystallite size by Scherrer analysis. Reliable crystal size estimation requires careful corrections for the instrumental width, and an instrumental width which is not much broader than the true peak width.

ESR

The ESR experiments were performed using a Bruker Elexsys E500 spectrometer operating at 9.88 GHz (X-band). All ESR spectra were obtained in dark and at room temperature. The Spin Counting tool in Xenon software was used to determine the spin density of PEDOT samples after a factory calibration of the cavity response function. The uncertainty of the spin concentration was estimated to be within ~10% and was verified by repeated measurements of a calibration sample (alanine pill).The calculation of the density of spin per monomer is based on the structural model for PEDOT-Tos proposed by K.E.Aasmundtveit et. al(*7*). ENREF 35 where the unit cell has a volume equal to $7{,}42*10^{-19}$ mm^3. Each unit cell consists of four EDOT monomers and one tosylate counter-ion. Consequently, one monomer occupies approximately a volume V_{EDOT} of $1{,}855*10^{-19}$ mm^3. The results of photoelectron spectroscopy measurements on PEDOT-PSS reveals PEDOT-PSS is composed of one EDOT

monomer every 3.8 PSS monomer. For pristine PEDOT-PSS, the spin density is measured to be $3.27*10^{16}$ spin/mm^3. Multiplying this number by V_{EDOT} and taking into account the factor of 3.8 (assuming the volume of EDOT is about the same as the volume of the PSS monomer), we obtain 0,023 spins per EDOT monomer. The same calculation for PEDOT-PSS with 0,05%, 0,5% and 5% DEG result in the following numbers: 0,0227, 0,0123, 0,0033 spin/monomer respectively.

Absorption spectroscopy and FTIR

Absorption spectra of PEDOT-Tos films were recorded on a Perkin Elmer Lambda 9 spectrophotometer from 300 to 1400 nm with a scan speed of 120 nm min^{-1} and a slit width of 1 nm. All the experiments are done at room temperature. Only visible range is shown in Fig S3a. The intensity of the spectra is normalized to account for film thickness difference and difference in average PEDOT density (higher PEDOT density in PEDOT-Tos than in PEDOT-PSS). In order to record the absorption in the far IR region, the FTIR spectra (Fig. S3b) of PEDOT-Tos film spin coated onto an IR window were recorded from 500-4000 cm^{-1} using FTIR spectrometer Equinox 55.

1. K.-C. Chang *et al.*, The Thermoelectric Performance of Poly(3,4-ethylenedi oxythiophene)/Poly(4-styrenesulfonate) Thin Films. *Journal of Elec Materi* **38**, 1182 (2009/07/01, 2009).
2. Y. Hiroshige, M. Ookawa, N. Toshima, Thermoelectric figure-of-merit of iodine-doped copolymer of phenylenevinylene with dialkoxyphenylenevinylene. *Synthetic Metals* **157**, 467 (2007).
3. X. Crispin *et al.*, The Origin of the High Conductivity of Poly(3,4-ethylenedioxythiophene)−Poly(styrenesulfonate) (PEDOT−PSS) Plastic Electrodes. *Chemistry of Materials* **18**, 4354 (2006/09/01, 2006).
4. K. Lee, A. J. Heeger, Y. Cao, Reflectance of polyaniline protonated with camphor sulfonic acid: Disordered metal on the metal-insulator boundary. *Physical Review B* **48**, 14884 (1993).
5. Y. Xia, A. G. MacDiarmid, A. J. Epstein, Camphorsulfonic Acid Fully Doped Polyaniline Emeraldine Salt: In situ Observation of Electronic and Conformational Changes Induced by Organic Vapors by an Ultraviolet/Visible/Near-Infrared Spectroscopic Method. *Macromolecules* **27**, 7212 (1994/11/01, 1994).
6. F. M. Smits, Measurement of sheet resistivities with the four-point probe. *the bell system technical journal*, 7 (1957).
7. K. E. Aasmundtveit *et al.*, Structure of thin films of poly(3,4-ethylenedioxythiophene). *Synthetic Metals* **101**, 561 (1999).